Human frataxin: iron and ferrochelatase binding surface†

Krisztina Z. Bencze,[a] Taejin Yoon,‡[b] César Millán-Pacheco,[c] Patrick B. Bradley,[a] Nina Pastor,[c] J. A. Cowan[b] and Timothy L. Stemmler*[a]

Received (in Cambridge, UK) 2nd March 2007, Accepted 19th March 2007
First published as an Advance Article on the web 28th March 2007
DOI: 10.1039/b703195e

The coordinated iron structure and ferrochelatase binding surface of human frataxin have been characterized to provide insight into the protein's ability to serve as the iron chaperone during heme biosynthesis.

Frataxin, a mitochondrial protein essential for cellular iron homeostasis, was recently implicated as the iron chaperone that delivers Fe(II) to enzyme partners during cellular heme and Fe–S cluster biosynthesis. Frataxin deficiency in humans is the cause of the neurodegenerative disorder Friedreich's ataxia (FRDA) affecting 1 in 50,000.[1] The trinucleotide repeat expansion in the first intron of the frataxin gene disrupts transcription, causing a frataxin deficiency that results in disruption of cellular iron homeostasis, progressive mitochondrial iron accumulation and a deficiency in heme and Fe–S clusters; the effects of these lead to a loss of cell viability and eventually patient death.[1,2] The iron binding ability of frataxin has been well documented,[3–5] with monomeric protein binding multiple iron atoms at micromolar binding affinities.[6–9] Frataxin binds at nanomolar affinity to the ferrochelatase and the iron–sulfur cluster (ISU) assembly apparatus, enzymes responsible for heme and Fe–S cluster bioassembly respectively.[6,7,10] Frataxin utilizes surface exposed helical plane residues to establish a binding interface with ferrochelatase.[5] Furthermore, the presence of frataxin stimulates *in vitro* assembly of both heme and Fe–S clusters.[6,7,11] Combined, these results suggest frataxin plays a direct role in Fe(II) delivery within the two separate Fe-cofactor production pathways.

Regarding the heme biosynthetic pathway, we have performed a detailed characterization of frataxin bound iron and the protein's ferrochelatase binding structure to provide additional insight into how frataxin delivers iron during Fe-cofactor production. We performed a spectroscopic characterization of the structure of iron bound to monomeric human frataxin, mapped ferrochelatase's intermolecular interface on frataxin and probed for probable structures of the complex between frataxin and ferrochelatase with the goal of enhancing our understanding of frataxin's activities as an iron chaperone. We recently characterized the structure of iron bound to monomeric yeast frataxin[8] and proposed a docking interaction of frataxin with the yeast ferrochelatase,[2] however the goal of this report was to confirm our understanding of these iron binding and transfer events in the more physiologically relevant human system. X-ray absorption spectroscopy (XAS) was utilized to examine the ligand coordination structure and oxidation state of iron bound to monomeric human frataxin. Nuclear magnetic resonance (NMR) spectroscopy was used to characterize frataxin residues at the ferrochelatase-binding interface. Finally, docking simulations were performed to simulate how frataxin binds and delivers iron to ferrochelatase. These results have provided a testable model for iron delivery during cellular heme biosynthesis.

XAS studies performed on iron loaded monomeric human frataxin were used to confirm the metal's oxidation state and metal–ligand coordination structure. Reproducible independent wild type frataxin XAS samples, covering residues 91–210, were prepared at 1 : 1 and 2 : 1 Fe(II) to protein ratios ([protein] = 3.3 mM in 50 mM HEPES (pH = 7.0), 3.5 mM TCEP, 40% glycerol).§ XANES edge energies for all samples are consistent with bulk iron existing in the ferrous oxidation state (Supporting Fig. 1). Simulations of the iron 1s → 3d transitions for both samples, showing dimensionless areas of 5.2 ± 0.5 and 4.8 ± 0.5 for 1 and 2 Fe bound, indicate that bound iron is maintained in a symmetric 6-coordinate Fe(II) ligand environment.[12] The 1s → 3d transition peak energies at 7122.5 and 7123.3 eV are consistent with high-spin Fe(II) in both samples.[12] Fourier transforms of the

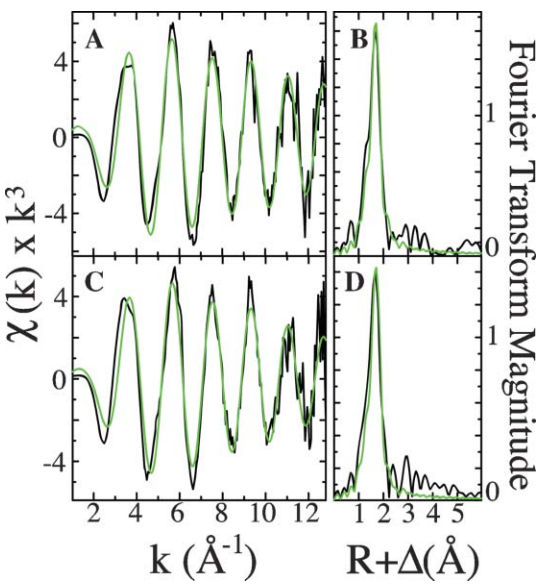

Fig. 1 EXAFS of frataxin bound iron. Raw EXAFS (black) and simulations (green) of 1 (A) and 2 (C) Fe bound. Fourier transforms of raw (black) and simulated (green) EXAFS of 1 (B) and 2 (D) Fe bound.

[a]*Department of Biochemistry and Molecular Biology, Wayne State University, School of Medicine, Detroit, MI 49201, USA. E-mail: tstemmle@med.wayne.edu*
[b]*Department of Chemistry, Ohio State University, Columbus, OH 43210, USA*
[c]*Facultad de Ciencias, Universidad Autónoma del Estado de Morelos, Cuernavaca, Morelos, México*
† Electronic supplementary information (ESI) available: XAS, NMR and docking data/analysis. See DOI: 10.1039/b703195e
‡ *Present address*: Department of Pediatrics, Stanford University, Stanford, California 94305, USA.

iron EXAFS (Fig. 1) indicate nearly symmetric nearest-neighbor ligand scattering environments at R < 2.5 Å and minimal long-range ordered scattering at R > 2.5 Å in both samples (Fig. 1). EXAFS fitting results confirm iron is constrained in a 6-coordinate oxygen/nitrogen based nearest neighbor ligand environment with average metal–ligand bond lengths centered at 2.12 Å (Supporting Table 1). A minimal improvement in our simulations were obtained upon inclusion of long-range (R > 2.8 Å) carbon scattering and there is no evidence for Fe···Fe scattering in iron loaded monomeric human frataxin.

NMR spectroscopy was used to identify the ferrochelatase binding surface on iron-loaded monomeric frataxin. Buffered iron was anaerobically added to ^{15}N-labeled frataxin in a capped NMR tube to achieve an oxygen free metal to protein stoichiometry of 1 : 1. Published binding studies report frataxin interacts with ferrochelatase at a 1 : 2 protein monomer stoichiometry.[7] In order to be consistent with known binding stoichiometries, we anaerobically added 2 equivalents of ferrochelatase to the iron loaded ^{15}N-labeled frataxin sample. All samples were initially buffer exchanged into 10 mM HEPES (pH = 7), 50 mM NaCl, 0.1% deoxycholate to prevent solution effects. ^{15}N filtered TROSY-HSQC spectra were used to monitor frataxin's amide chemical shift perturbations, first upon iron binding and then upon complexation of frataxin with ferrochelatase. Amide chemical shift perturbations coupled to complex formation were observed on frataxin's helical surface and strand-1 residues (Fig. 2). Similar results were observed for the yeast orthologs.[5] Frataxin's surface exposed helix-1 conserved residues (D104, E108 and E111) and conserved strand-1 residues (D122 and D124) showed appreciable chemical shift perturbations in the frataxin:ferrochelatase complex. Additional conserved helix-1 residues (D112, L113 and D115) were broadened during the iron titration beyond detection (Supporting Fig. 2), as previously observed.[4] Additional non-conserved helix-1 residues (F109 and A114), strand-1 residue S126 and helix-2 residues (K192, K195 and L197) also showed amide perturbations following complex formation. These data, along with published binding and molecular interface studies on the yeast and human orthologs, support the idea that monomeric frataxin interacts with the ferrochelatase dimer predominantly utilizing frataxin's helical surface, including iron binding residues in the helix-1/strand-1 conserved acidic residue patch of the protein.[4,5,7,10]

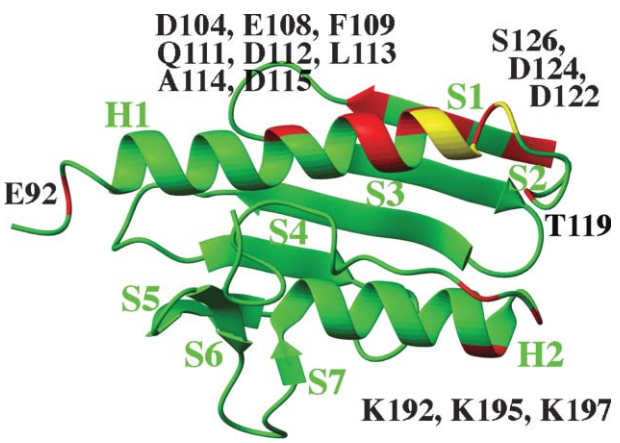

Fig. 2 Human frataxin residues perturbed at their amide position upon forming a complex with iron and ferrochelatase. Unshifted (green) and shifted (red) residues identified on the apo-protein's structure. Yellow residues are line broadened beyond recognition resulting from Fe binding.

Docking simulations performed using ZDOCK[13] place monomeric frataxin in an orientation that promotes iron delivery to the ferrochelatase dimer (Fig. 3). Published structures of apo-human frataxin and Co^{2+} loaded human ferrochelatase were used to structurally simulate docking.[14,15] Rigorous selection criteria, determined from published structural and biochemical details of frataxin and ferrochelatase's initial iron binding residues, were employed when identifying the best possible complex structure. The first selection criterion took into account that human ferrochelatase is reported to initially bind iron using residues H230, H231 and D383, located opposite to the membrane binding side of the molecule (Fig. 4).[15] Iron is then directed down the substrate channel lined with Trp, Tyr and Arg residues until it reaches the protein's active site near the membrane surface (identified as the yellow oval in Fig. 3). The second selection criterion utilized published data on the yeast ortholog[5] and data in this report identified that frataxin binds ferrochelatase utilizing its helical surface residues. Others and we have identified frataxin's iron binding site on the protein's helix-1,[4,5,8,16] a component region at frataxin's intermolecular interface with ferrochelatase. Therefore, a third selection criterion was that frataxin's helix-1 iron binding site had to be close to ferrochelatase's initial metal binding or "acceptance" site. Finally, a monomeric protein stoichiometry of 1 : 2 for frataxin to ferrochelatase has been reported,[7,10] so the final selection criterion for a possible structure included this condition. The lowest energy complex structure from our simulations suggests iron-loaded monomeric frataxin docks on the exposed matrix side of ferrochelatase in the region where the enzyme initially accepts iron. Frataxin's iron binding helix-1 residues D112 and D115 are within 9 Å of ferrochelatase molecule 2's initial metal binding residues H230, H231 and D383 in the best

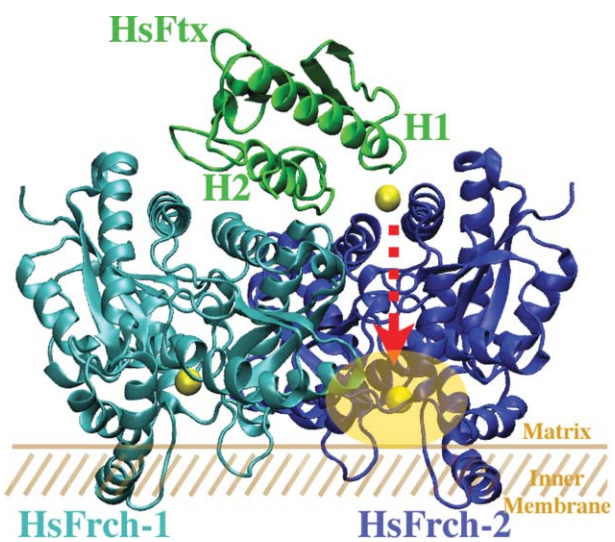

Fig. 3 Docking simulation of frataxin (Ftx) (green) with the ferrochelatase (Frch) dimer. Frataxin interacts with ferrochelatase on the matrix exposed side of the protein dimer during iron delivery (yellow ball). Delivered iron would then be available to be transported down ferrochelatase's substrate channel (red arrow) towards the enzyme's active site (yellow oval) located on the membrane side of the molecule.

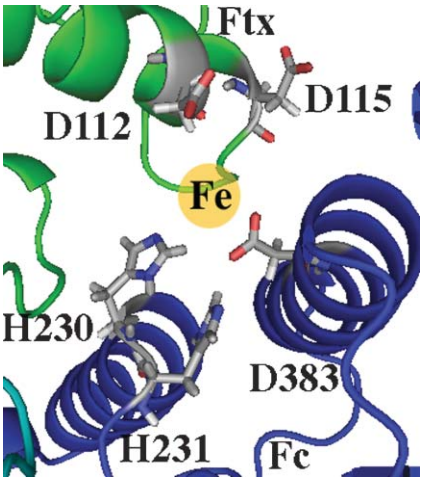

Fig. 4 Expanded view of metal binding residues at the proposed frataxin (green)/ferrochelatase molecule 2 (blue) interface.

simulated complex (Fig. 4). This complex structure places iron, delivered by frataxin, in an orientation so that metal can first be accepted by ferrochelatase. Ferrochelatase bound iron would then be free to be transferred down the protein's substrate channel, eventually reaching the enzyme's active site (red arrow and yellow oval, respectively in Fig. 3).

In conclusion, a combination of XAS and NMR studies was used to confirm that monomeric frataxin binds high spin ferrous iron in a six-coordinate metal–ligand coordination environment utilizing in part carboxylate oxygens as ligands from conserved acidic residues in frataxin's helix-1. Additional NMR studies confirm frataxin's ferrochelatase docking surface is constructed predominantly by helical surface residues on the protein's helical face. Docking simulations were used to generate a model of how iron-loaded monomeric frataxin docks to the ferrochelatase dimer. Complex formation in this manner would allow for metal delivery between the two protein partners, providing the ferrous iron required for *in vivo* heme biosynthesis. Mutational and structural experiments, directed at testing our model for frataxin/ferrochelatase binding, are currently in progress.

This work was supported by the National Institute of Diabetes and Digestive and Kidney Diseases R01DK068139 (TLS) and by the National Science Foundation CHE-0111161 (JAC).

Notes and references

§ **General chemicals**. HEPES, TCEP, deoxycholate, glycerol and NaCl were purchased from Sigma (St. Louis, MO). **Protein purification**. Purification and concentration quantification of human frataxin and ferrochelatase followed published protocols.[7] **NMR spectroscopy**. NMR experiments were performed on a Varian Inova 600 MHz spectrometer operating with a triple resonance cold probe. **XAS experiments**. XAS studies were carried out at both the Stanford Synchrotron Radiation Laboratory (SSRL), on beamline 9-3, and the National Synchrotron Light Source (NSLS), on beamline X9b. SSRL is a national user facility operated by Stanford University on behalf of the U.S. Department of Energy, Office of Basic Energy Sciences. The SSRL Structural Molecular Biology Program is supported by the Department of Energy, Office of Biological and Environmental Research, and by the NIH, National Center for Research Resources, Biomedical Technology Program. NSLS, located at Brookhaven National Laboratory, is supported by the U.S. Department of Energy, Division of Materials Sciences and Division of Chemical Sciences, under Contract No. DE-AC02-98CH10886. Spectra were collected on multiple reproducible samples. Data collection and analysis protocols have been previously reported.[8]

1 M. B. Delatycki, R. Williamson and S. M. Forrest, *J. Med. Genet.*, 2000, **37**, 1–8.
2 K. Z. Bencze, K. C. Kondapalli, J. D. Cook, S. McMahon, C. Millan-Pacheco, N. Pastor and T. L. Stemmler, *Crit. Rev. Biochem. Mol. Biol.*, 2006, **41**, 269–291.
3 J. Adamec, F. Rusnak, W. G. Owen, S. Naylor, L. M. Benson, A. M. Gacy and G. Isaya, *Am. J. Hum. Genet.*, 2000, **67**, 549–562.
4 M. Nair, S. Adinolfi, C. Pastore, G. Kelly, P. Temussi and A. Pastore, *Structure (Cambridge, MA, U. S.)*, 2004, **12**, 2037–2048.
5 Y. He, S. L. Alam, S. V. Proteasa, Y. Zhang, E. Lesuisse, A. Dancis and T. L. Stemmler, *Biochemistry*, 2004, **43**, 16254–16262.
6 T. Yoon and J. A. Cowan, *J. Am. Chem. Soc.*, 2003, **125**, 6078–6084.
7 T. Yoon and J. A. Cowan, *J. Biol. Chem.*, 2004, **279**, 25943–25946.
8 J. D. Cook, K. Z. Bencze, A. D. Jankovic, A. K. Crater, C. N. Busch, P. B. Bradley, A. J. Stemmler, M. R. Spaller and T. L. Stemmler, *Biochemistry*, 2006, **45**, 7767–7777.
9 F. Bou-Abdallah, S. Adinolfi, A. Pastore, T. M. Laue and N. D. Chasteen, *J. Mol. Biol.*, 2004, **341**, 605–615.
10 E. Lesuisse, R. Santos, B. F. Matzanke, S. A. Knight, J. M. Camadro and A. Dancis, *Hum. Mol. Genet.*, 2003, **12**, 879–889.
11 S. Park, O. Gakh, H. A. O'Neill, A. Mangravita, H. Nichol, G. C. Ferreira and G. Isaya, *J. Biol. Chem.*, 2003, **278**, 31340–31351.
12 T. E. Westre, P. Kennepohl, J. G. DeWitt, B. Hedman, K. O. Hodgson and E. I. Solomon, *J. Am. Chem. Soc.*, 1997, **119**, 6297–6314.
13 R. Chen, L. Li and Z. Weng, *Proteins: Struct., Funct., Genet.*, 2003, **52**, 80–87.
14 G. Musco, G. Stier, B. Kolmerer, S. Adinolfi, S. Martin, T. Frenkiel, T. Gibson and A. Pastore, *Structure (Cambridge, MA, U. S.)*, 2000, **8**, 695–707.
15 C. K. Wu, H. A. Dailey, J. P. Rose, A. Burden, V. M. Sellers and B. C. Wang, *Nat. Struct. Biol.*, 2001, **8**, 156–160.
16 O. Gakh, S. Park, G. Liu, L. Macomber, J. A. Imlay, G. C. Ferreira and G. Isaya, *Hum. Mol. Genet.*, 2006, **15**, 467–479.